https://doi.org/10.1093/plphys/kiad275 PLANT PHYSIOLOGY 2023: 1–16

Plant Physiology®

Research Article

Bicarbonate activation of the monomeric photosystem II-PsbS/Psb27 complex

Andrea Fantuzzi [1,†], Patrycja Haniewicz [2,3,†], Domenica Farci [4], M. Cecilia Loi [5], Keunha Park [1], Claudia Büchel [6], Matthias Bochtler [3,7], A. William Rutherford [1,*,‡] and Dario Piano [3,5,‡]

1 Department of Life Sciences, Imperial College London, London SW7 2AZ, UK
2 Department of Plant Physiology, Warsaw University of Life Sciences - SGGW, Warsaw 02-776, Poland
3 Laboratory of Structural Biology, International Institute of Molecular and Cell Biology, Warsaw 02-109, Poland
4 Department of Chemistry, Umea University, 90187 Umea, Sweden
5 Department of Life and Environmental Sciences, University of Cagliari, Cagliari 09123, Italy
6 Institute of Molecular Biosciences, University of Frankfurt, Frankfurt am Main 60438, Germany
7 Polish Academy of Science, Institute of Biochemistry and Biophysics, Warsaw 02-106, Poland

*Author for correspondence: a.rutherford@imperial.ac.uk
†These authors contributed equally.
‡Senior author.
The author responsible for distribution of materials integral to the findings presented in this article in accordance with the policy described in the Instructions for Authors (https://academic.oup.com/plphys/pages/General-Instructions) is Dario Piano (dario.piano@unica.it).

Abstract

In thylakoid membranes, photosystem II (PSII) monomers from the stromal lamellae contain the subunits PsbS and Psb27 (PSIIm-S/27), while PSII monomers (PSIIm) from granal regions lack these subunits. Here, we have isolated and characterized these 2 types of PSII complexes in tobacco (*Nicotiana tabacum*). PSIIm-S/27 showed enhanced fluorescence, the near absence of oxygen evolution, and limited and slow electron transfer from Q_A to Q_B compared to the near-normal activities in the granal PSIIm. However, when bicarbonate was added to PSIIm-S/27, water splitting and Q_A to Q_B electron transfer rates were comparable to those in granal PSIIm. The findings suggest that the binding of PsbS and/or Psb27 inhibits forward electron transfer and lowers the binding affinity for bicarbonate. This can be rationalized in terms of the recently discovered photoprotection role played by bicarbonate binding via the redox tuning of the $Q_A/Q_A^{\bullet-}$ couple, which controls the charge recombination route, and this limits chlorophyll triplet-mediated $^1O_2$ formation. These findings suggest that PSIIm-S/27 is an intermediate in the assembly of PSII in which PsbS and/or Psb27 restrict PSII activity while in transit using a bicarbonate-mediated switch and protective mechanism.

Introduction

Oxygenic photosynthesis is a light-driven biochemical process providing the biosphere with organic carbon, energy, and molecular oxygen (Johnson 2016). In land plants, this process takes place in the chloroplast, a specialized organelle consisting of outer and inner membranes forming a network of photosynthetic membranes named thylakoids (Albertsson 2001; Vothknecht and Westhoff 2002). The protein composition of the different portions of these membranes is distinct, showing segregation of the photosystems. Photosystem II (PSII) is mainly present in the appressed granal regions, while photosystem I (PSI) is found in the nonappressed regions of the granal margins and in the stromal lamellae (Andersson and Anderson 1980). Dynamic responses to various environmental factors have been shown to change the ultrastructure and composition of the membranes and photosystems (Ruban and Johnson 2015; Kirchhoff 2019).

In land plants, the organization of thylakoid membranes also reflects the partition of different kinds of PSII, which are assembled and repaired in the stromal lamellae, while the fully

Received March 09, 2023. Accepted April 05, 2023. Advance access publication May 18, 2023

Open Access

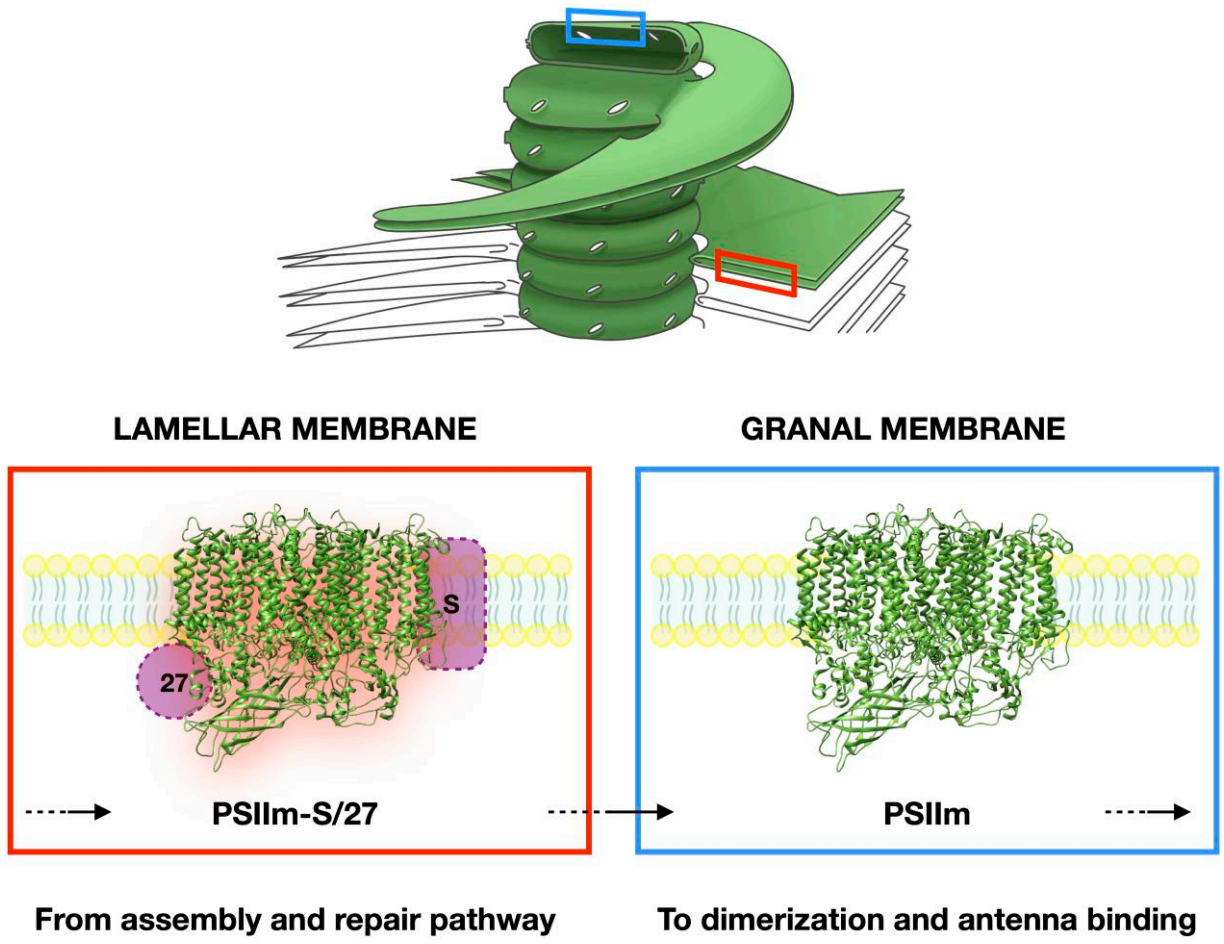

Figure 1. The location within the thylakoid membrane of the protein complexes investigated in this work. PSIIm-S/27 is in the lamellar membranes (left inset) and suggested to be an intermediate in the assembly and repair pathway, probably after photoactivation. In this model, PSIIm-S/27 the complex migrates (as indicated by the black arrows) to the grana membranes (right inset) where, upon dissociation of PsbS and Psb27, it forms the active monomer, PSIIm. The PSIIm then forms active dimers and binds antenna proteins to form fully functional complexes.

functional PSII complexes are located in the grana (Andersson and Anderson 1980; Danielsson et al. 2006) (Fig. 1). The small fraction of PSII complexes that are found in stromal lamellae are mainly PSII monomers (PSIIm) and a series of smaller assembly intermediates. In contrast, the grana are dominated by PSII dimers that can form a range of complexes with chlorophyll antenna proteins, including Light Harvesting Complex II (LHCII), forming PSII-LHCII (Danielsson et al. 2006; Watanabe et al. 2009; Haniewicz et al. 2013).

PSII, the water/plastoquinone photo-oxidoreductase, uses the energy of light to drive charge separation, oxidize water, and reduce plastoquinone. The photochemistry occurs as a 1-photon/1-electron reaction 4 times sequentially to accumulate the 4 oxidizing equivalents necessary for water oxidation and oxygen release at the Mn_4CaO_5 active site on the luminal side of PSII (Dau and Zaharieva 2009). An exchangeable quinone, Q_B, accepts 2 electrons and 2 protons sequentially, before it is released as Q_BH_2 from the stromal side of PSII into the PQ/PQH_2 pool in the membrane (De Causmaecker et al. 2019). The sequential electron transfer steps involve the formation of a stable intermediate, $Q_B^{\bullet-}$, that can back-react via $Q_A^{\bullet-}$ with the semistable, charge accumulation intermediates of the Mn_4CaO_5 cluster (Rutherford et al. 1982). This back reaction occurs via the thermal repopulation of the $P^{\bullet+}Pheo^{\bullet-}$ state, which recombines mainly by a route forming the chlorophyll triplet state $^3P_{680}$ (Rutherford et al. 1981). This triplet state reacts with oxygen to form singlet-oxygen $^1O_2$ (Krieger-Liszkay 2005; Rutherford et al. 2012). The $^1O_2$ generated causes damage to PSII (Krieger-Liszkay 2005). Other reactive oxygen species, generated by reductive and oxidative processes in PSII, might also contribute to damage (Pospíšil 2016).

Repairing the damage is an energetically costly process since proteins and cofactors must be synthesized and replaced to maintain efficient photosynthetic activity (Komenda et al. 2012; Tikkanen and Aro 2012). This takes place in the stromal lamellae via a stepwise assembly of subcomplexes (Komenda et al. 2012; Nickelsen and Rengstl 2013; Puthiyaveetil et al. 2014; Tomizioli et al. 2014). A large variety of PSII protein complexes are present in the stroma lamellae, with partially assembled systems coexisting with the PSII in different oligomeric states and different levels of activity

(Danielsson et al. 2006; Haniewicz et al. 2013; Puthiyaveetil et al. 2014; Tomizioli et al. 2014). Inactive PSII from the stromal lamellae have been studied for decades (Melis 1985; Lavergne and Leci 1993), and it was reported that 10% to 20% of PSII in the chloroplast were inactive and this was due to blocked forward electron transfer and not due to a lack of oxidized plastoquinone (Lavergne and Leci 1993).

The complexity of the assembly/repair cycle, together with the low abundance of most of the intermediate complexes, means that our understanding of it is still evolving (Komenda et al. 2012; Nickelsen and Rengstl 2013). Due to the low concentration, instability, and intrinsically transient nature of these assembly intermediates, their isolation has required specific strategies: (i) the generation of mutants that lack either specific assembly factors or small PSII subunits, resulting in the accumulation of assembly intermediates (Komenda et al. 2002; Roose and Pakrasi 2008; Huang et al. 2021; Zabert et al. 2021) and/or (ii) tagging 1 of the PSII subunits to allow isolation of low concentration intermediates by affinity chromatography (Nowaczyk et al. 2006; Liu et al. 2011a). Differential fractionation (Danielsson et al. 2006) and more recently differential solubilization (Haniewicz et al. 2013; Fey et al. 2008) allowed the isolation of some of the subpopulations of PSII. Fractions originating from the lamellae and the granal margins (Haniewicz et al. 2013, 2015) yielded a monomeric PSII containing 2 additional subunits, PsbS and Psb27, which are absent in functional granal PSII (Haniewicz et al. 2015). While Psb27 has been shown to bind to PSII subcomplexes and to play a role in PSII assembly (Nowaczyk et al. 2006; Roose and Pakrasi 2008), PsbS has been associated, directly or indirectly, with photoprotection mechanisms via nonphotochemical fluorescence quenching (Niyogi and Truong 2013; Ruban 2016; Bassi and Dall'Osto 2021).

Since its discovery in 1984 (Ljungberg et al. 1984), the role of PsbS has been controversial (Niyogi and Truong 2013; Fan et al. 2015; Ware et al. 2015; Ruban 2016; Dall'Osto et al., 2017; Bassi and Dall'Osto 2021). Despite the availability of a PsbS crystallographic structure (Fan et al. 2015), there is still a debate about its basic components. The presence of chlorophyll and xanthophyll (Correa-Galvis et al. 2016; Gachek et al. 2019) and its role as a luminal pH sensor (Bergantino et al. 2003; Li et al. 2004; Roach and Krieger-Liszkay 2012; Liguori et al. 2019) are still debated. The primary role of PsbS is thought to be a protective one, as a key player in some aspects of nonphotochemical quenching (NPQ) (Niyogi and Truong 2013; Ruban 2016; Bassi and Dall'Osto 2021). Several reports showed the involvement, either direct or indirect, of PsbS, in quenching the excess of energy in free LHCII complexes and/or in LHCIIs associated with PSII (Sacharz et al. 2017). A photoprotective role has also been suggested to act via CP47 and the minor external antennas of PSII (Correa-Galvis et al. 2016). However, to date, there is no consensus on a mechanism linking PsbS with NPQ and the xanthophyll cycle that would explain PsbS-mediated photoprotection and its role as a pH sensor.

PsbS has been found to be bound stoichiometrically to purified PSII cores only in samples originating from the lamellae and granal margins of *Nicotiana tabacum* thylakoids (Haniewicz et al. 2013). Indirect evidence of its presence in PSII dimers and monomers and its association to the PSII-LHCII complexes in grana have also been reported (Bergantino et al. 2003; Caffarri et al. 2009; Correa-Galvis et al. 2016).

Psb27 is present in eukaryotes and prokaryotes, though most of the information relates to the cyanobacterial form. Important differences, such as the eukaryotic Psb27 lacking the covalently bound lipid moiety that is present in the cyanobacteria, raise doubts on whether they have the same location and function. In cyanobacteria, Psb27 is involved in the assembly of the Mn_4CaO_5 cluster and was found to be associated with inactive PSII lacking the 3 extrinsic proteins, PsbO, PsbU, and PsbV (Roose and Pakrasi 2004; Nowaczyk et al. 2006). It was found to play an important role during PSII D1 repair, where it was suggested to bind to CP43 and facilitate the assembly of the Mn cluster by providing greater accessibility and preventing premature association of the other extrinsic proteins (Nowaczyk et al. 2006; Roose and Pakrasi 2008). Its location close to the CP43 loop E and its allosteric role in preventing the binding of the extrinsic proteins (Liu et al. 2011a, 2011b) were confirmed in 2 recent cryo-EM structures (Huang et al. 2021; Zabert et al. 2021). Its role in facilitating the photoactivation of the Mn cluster was found to be more complex than simply displacing the extrinsic proteins from the apo-PSII (Avramov et al. 2020). In land plants, this subunit is found to exist in 2 isoforms, Psb27-1 and Psb27-2 (Chen et al. 2006; Wei et al. 2010). Their specific function is still under investigation, with Psb27-1 found not only to be required for the efficient repair of photodamaged PSII (Chen et al. 2006) but also to play a role in the state transition mechanism (Dietzel et al. 2011), while Psb27-2 is suggested to play an important role in the processing of the precursor form of D1 (Wei et al. 2010).

In the present study, we have characterized a PSIIm containing PsbS and Psb27, which was isolated from the stromal lamellae and the grana margins (PSIIm-S/27) from tobacco (*N. tabacum* L.). We compared this complex with the PSIIm isolated from the grana stacks (PSIIm). The data indicate an unexpected role for PsbS and/or the Psb27 protecting newly assembled and photoactivated PSII by inhibiting electron transfer, an inhibition that is reversed by bicarbonate binding.

Results

Association of PsbS and Psb27 to PSIIm

Two types of purified PSII core complexes, PSIIm and the PSIIm-S/27, were isolated from *N. tabacum* L. according to the procedures previously described in Haniewicz et al. (2013, 2015), where it was demonstrated that the PSIIm and the PSIIm-S/27 originate from the grana stacks and margins/stromal lamellae, respectively (Fig. 1). The 2 types of

monomeric PSII were compared by SDS–PAGE, and we confirmed the previous observations obtained in the previous detailed work, which used SDS–PAGE, mass spectrometry, and western blots (Haniewicz et al. 2013, 2015). A table collating the information from the mass spectrometry is shown in Supplemental Table S1.

The SDS–PAGE showed that the samples had similar composition in terms of protein subunits, except for the 2 additional bands in the PSIIm-S/27 at 20 and 13 kDa (Figs. 2A and S1, bands 11 and 13), attributed to the PsbS and Psb27 subunits, respectively (Haniewicz et al. 2013; Supplemental Table S1). Based on these results, the most substantial difference between the 2 samples is the presence of the subunits PsbS and Psb27 in the PSIIm-S/27. We note that PSIIm also seems to lack the small subunits PsbJ, PsbQ, and PsbP, based on the SDS–PAGE and the mass spectrometry. We, nevertheless, consider that these differences are due to an artifactually low level of detection of these subunits in the mass spectrometry and SDS–PAGE data, because western blot analysis, performed and published in our previous work (Haniewicz et al. 2013, 2015), indicated that these subunits were present. However, this could reflect partial loss of these subunits in the PSIIm sample and would be consistent with the observation that this sample is much less stable than the PSIIm-S/27. In contrast, the PsbS and Psb27 subunits could not be detected in the PSIIm sample by any of the 3 methods.

Semiquantitative mass spectrometry analysis provided some indications on the relative abundance of the different subunits (Supplemental Table S1). Overall, their abundance is lower than the 5 main subunits but higher than the abundance of PsbP and PsbQ, which were shown to be present by western blot. Fractional losses of PsbS and Psb27 subunits could have occurred during isolation of the protein complex resulting in a degree of sample heterogeneity (as is seen in the functional characterization below), but despite this, their abundance is high enough to consider them as being quasi-stoichiometric in the PSII core complexes. The SDS–PAGE and mass spectrometry data indicate that monomeric PsbS is bound in PSIIm-S/27 (Supplemental Fig. S1 and Table S1). Finally, in the SDS–PAGE, at masses higher than 45 kDa, the pattern of bands for each of the 2 samples shows quantitative differences. However, these bands are not directly related with PSII and appear to be copurified components identified based on the mass spectrometry analysis as glycine dehydrogenase, V-type proton ATPase, and the β-subunit of mitochondrial ATPase (Supplemental Fig. S1 and Table S1). Small differences in the substoichiometric content of external antenna proteins, which are mainly ascribed to CP26 and CP29, were also observed (Supplemental Table S1).

Spectroscopic characterization of PSIIm and the PSIIm-S/27

UV-Vis absorption spectra of the PSIIm and the PSIIm-S/27 were recorded (Fig. 2B). When normalizing the spectra at 675 nm, the comparison showed only minimal differences localized between 350 and 550 nm with the PSIIm-S/27 showing slightly higher absorbance. As the Psb27 and PsbS have been shown to contain no chromophores, these differences are more likely to be due to the small differences in CP26 and CP29 content of the samples (see Supplemental Text S1). It is of note that a chlorophyll molecule was reported to be present at the interface between the 2 monomers in the crystal structure of PsbS (Fan et al. 2015). However, this chlorophyll was bound via nonspecific hydrophobic interactions could well be an artifact of the purification (Fan et al. 2015). Fan et al. (2015) stated that each PsbS subunit adopts a folding pattern that precluded the binding of chlorophyll and carotenoid chromophores in the locations where these pigments bind canonical LHC proteins.

Room temperature fluorescence emission spectra were recorded for both PSII samples and showed a single peak at 681 and 682.5 nm for PSIIm-S/27 and PSIIm, respectively (Fig. 2C). In equally concentrated samples, the intensity of the emission peak was much higher (nearly double) for the PSIIm-S/27 sample when compared with the PSIIm (Fig. 2C).

The comparison of the circular dichroism (CD) spectra (Fig. 2D) for the PSIIm and the PSIIm-S/27 samples showed differences that can be related to the small changes in the absorption spectra shown in the Fig. 2B. Overall, both spectra resemble a typical PSII spectrum (Alfonso et al. 1994; Krausz et al. 2005), suggesting that no major changes in the position or number of the cofactors is induced by the presence of PsbS and Psb27. However, in the PSIIm-S/27 sample, the spectral region between 350 and 550 nm showed changes in peak intensity and position, with 3 minor bands at 427, 475, and 484 nm, respectively. The Qy band showed the typical PSII double peak in both samples (Alfonso et al. 1994; Krausz et al. 2005). In the PSIIm-S/27 sample, these features were red-shifted by about 2 nm with respect to PSIIm (Fig. 2D).

Water oxidation catalytic activity

The enzymatic activities of both PSIIm and PSIIm-S/27 were compared by measuring their oxygen evolution rates. PSIIm showed good activity with rates of 1030 ± 13 μmol O_2 mg Chl^{-1} h^{-1}. In contrast, PSIIm-S/27 showed a drastically reduced activity of 52 ± 5 μmol O_2 mg Chl^{-1} h^{-1} (Table 1).

Electron transfer from $Q_A^{\bullet-}$ to Q_B or $Q_B^{\bullet-}$

PSII photochemistry was tested by measuring flash-induced chlorophyll fluorescence and $Q_A^{\bullet-}$ oxidation kinetics. The illumination with a single-saturating flash of a dark-adapted sample induces the reduction of Q_A to $Q_A^{\bullet-}$ in most of the centers, with a resulting increase in the prompt fluorescence yield. Subsequent reoxidation of $Q_A^{\bullet-}$, either by electron transfer to Q_B or $Q_B^{\bullet-}$ or by recombination with S_2, results in the decay of the fluorescence yield (Crofts and Wraight 1983).

Figure 3A shows that both minimal fluorescence (F_0) and maximal fluorescence (F_m) yields were higher in the

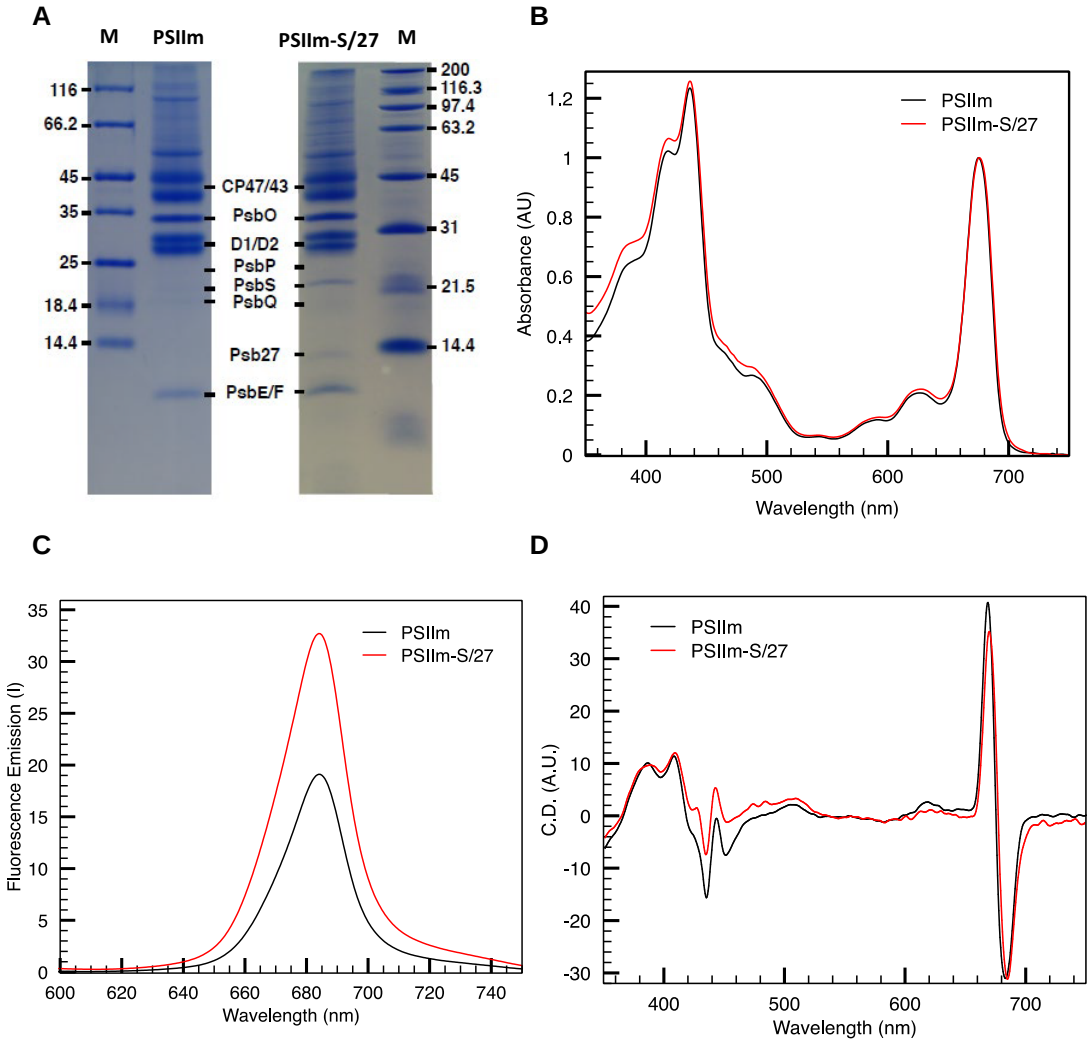

Figure 2. Comparisons of the PSIIm and PSIIm-S/27. **A)** Coomassie Blue Stained SDS–PAGE of the PSIIm and PSIIm-S/27. The additional presence of a ∼22-kDa (PsbS) band and a ∼14-kDa (Psb27) band in the PSIIm-S/27 sample is indicated together with the main PSII subunits. The lanes labeled as M indicate the molecular weight markers. **B)** UV-Vis absorption spectra of PSIIm (black line) and PSIIm-S/27 (red line). Spectra were taken at 20 °C in buffer A and were normalized at 675 nm. **C)** Fluorescence emission spectra of PSIIm (black line) and PSIIm-S/27 (red line). Spectra, recorded at 4 °C in buffer A with excitation at 437 nm. **D)** CD spectra at 20 °C in buffer A of PSIIm-S/27 (red line) and PSIIm (black line).

Table 1 Rates of oxygen evolution for PSIIm and PSIIm-S/27 with or without added bicarbonate.

PSII type	Added [$NaHCO_3$]	Oxygen evolution rates (μmol O_2/mg Chl^{-1} h^{-1})
PSIIm	0	1,030 ± 13
	5 mM	1,182 ± 10
PSIIm-S/27	0	52 ± 5
	5 mM	795 ± 8

Data represent mean ± SD, $n = 3$. The value reported for PSIIm with $NaHCO_3$ agrees with an earlier report (Piano et al. 2010).

PSIIm-S/27 sample (see Supplemental Text S2). PSIIm was found to be unstable during the measurements at room temperature; therefore, experiments were performed at 15 °C (Fig. 3, B and D). This is likely to slow down some rates when compared to other measurements done at room temperature and when comparing them to the literature. The decay rates of the fluorescence yield are shown in Fig. 3B. PSIIm kinetics are like those expected for functional PSII, while in PSIIm-S/27, the fluorescence decayed ∼10 times more slowly, indicating a marked inhibition of forward electron transfer. The kinetics were fitted with 3 decay phases (Fig. 3B and Table 2), and the origins of the decay phases were assigned to forward and backward electron transfer reactions according to the literature (Vass et al. 1999).

The initial fast phase arises from $Q_A^{\bullet-}$ forward electron transfer to either Q_B or $Q_B^{\bullet-}$. It has a rate of 1.9 ms and an amplitude of 31% for the PSIIm but a drastically reduced rate and amplitude of 17 ms and 7% amplitude for PSIIm-S/27.

The middle phase is often assigned to be electron transfer from $Q_A^{\bullet-}$ when the Q_B site is either empty or occupied by

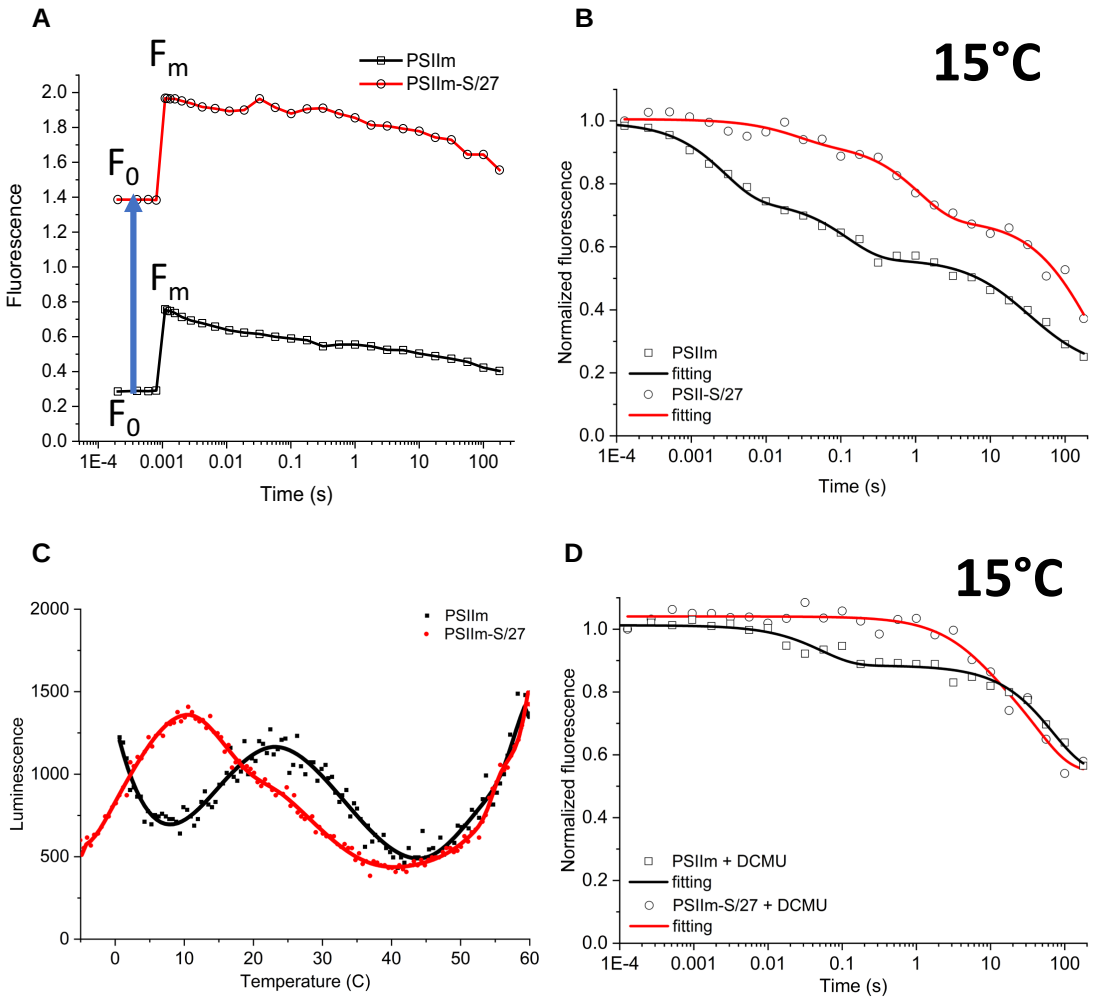

Figure 3. Fluorescence measurements of the PSIIm and PSIIm-S/27 complexes. **A)** Fluorescence relaxation kinetics data presented without normalization to show the values of F_0 and F_m for PSIIm (squares symbols, black line) and PSIIm-S/27 (circles symbols, red line). Both F_0 and F_m were found to be higher in the sample with bound PsbS and Psb27. **B)** Fluorescence relaxation kinetics of PSIIm (squares, black line) and PSIIm-S/27 (circles, red line), measured at 15 °C in buffer A. Data were normalized using the initial amplitudes. Fittings were carried out with equation 1 (see Materials and methods). **C)** TL measurements for PSIIm (black squares and line) and PSIIm-S/27 (red circles and line), in buffer A. Single saturating flash was given at 5 °C followed by rapid cooling to −5 °C. Scan rate was 0.5 °C/s. **D)** Fluorescence relaxation kinetics upon a single saturating flash for the PSIIm (squares, black line) and PSIIm-S/27 (circles, red line), measured at 15 °C in buffer A in the presence of 10 μM DCMU. Data were normalized using the initial amplitudes. Fittings were carried out with Eq. 1 (see Materials and methods).

Table 2 Kinetic parameters of flash-induced chlorophyll fluorescence decay in PSIIm, PSIIm-S/27 samples in absence or presence of additional bicarbonate in solution

			Fast phase		Middle phase		Slow phase	
PSII type	Added $NaHCO_3$ [mM]	T °C	*t* (ms)	Amp (%)	*t* (ms)	Amp (%)	*t* (s)	Amp (%)
PSIIm	0	15	1.9 ± 0.3	31 ± 2	85 ± 10	18 ± 3	23 ± 4	51 ± 1
PSIIm-S/27	0	15	17 ± 3	7 ± 3	770 ± 40	25 ± 3	180 ± 35	68 ± 2
	0	20	67 ± 10	21 ± 4	982 ± 130	34 ± 2	41 ± 5	45 ± 3
	5	20	3 ± 0.5	27 ± 2	115 ± 21	25 ± 2	13 ± 2	48 ± 2
PSII monomer(*)	0	20	3.7 ± 0.5	30 ± 7	37 ± 15	11 ± 2	9.9 ± 0.7	59 ± 5

The values of the kinetic half-lives (*t*) and the amplitudes of each phase are compared to the literature values for PSII monomer from *T. elongatus* (Zimmermann et al. 2006) (*). Data represent mean ± SD, $n = 3$.

Q_BH_2 at the time of the flash, and therefore the electron transfer rate is determined by the arrival of PQ into the Q_B site. For PSIIm, this phase shows an amplitude of 18% and a halftime of 85 ms, kinetics compatible with the usual assignment of this phase although on the slow side of the range, and could indicate a contribution to this phase of charge recombination with $TyrZ^{\bullet}$ in damaged centers. However, for PSIIm-S/27, while the amplitude is like that in

PSIIm, the decay is 9-fold slower, with a $t_{1/2} = 770$ ms. This is a very slow value for quinone exchange although slow quinone exchange is a feature of bicarbonate loss from the non-heme iron or bicarbonate replacement by other carboxylic acids (Shevela et al. 2012). This range of fluorescence decay is within those seen for S_2 recombination with $Q_A^{\bullet-}$ in PSIIm (Zimmermann et al. 2006), but it seems that in this material and at this temperature, this $S_2Q_A^{\bullet-}$ recombination takes place more slowly (see below).

The third and slowest phase is usually attributed to the back reaction of $Q_A^{\bullet-}$ with the S_2 state of the Mn cluster, and thus this phase is seen when forward electron transfer is blocked due to reduction of the pool, modification of the Q_B site, or binding of a herbicide in the Q_B site. This phase with a $t_{1/2} = 23$ s seems to be present in about half of the centers in PSIIm; this is in common with other reports from PSIIm in the literature (Table 2). The slower rates compared with the literature values are due to the lower temperature (15 °C) used here. The PSIIm-S/27 sample showed even more of this phase, 68%, and a marked slowdown of the half-time to 180 s. Thermoluminescence (TL) measurements of PSIIm showed that upon a single saturating flash, the PSIIm presents a single peak at 22 °C while PSIIm-S/27 presents a peak at 10 °C with a shoulder at 25 °C (Figs. 3C and S2). These peaks may be attributed to $S_2Q_B^{\bullet-}$ and $S_2Q_A^{\bullet-}$ recombination respectively based on the typical TL peak temperatures (Rutherford et al. 1982). The TL data suggest that the presence of PsbS and/or Psb27 blocks the electron transfer from $Q_A^{\bullet-}$ to Q_B. This appears to agree with fluorescence kinetics presented above on the $Q_A^{\bullet-}$ reoxidation kinetics considering the temperature of the measurement.

Effect of the inhibitor DCMU on the $Q_A^{\bullet-}$ oxidation kinetics

To investigate the possible interference of PsbS and/or Psb27 with Q_B binding, we measured the fluorescence yield relaxation kinetics in the presence of the PSII inhibitor DCMU (Fig. 3D). This inhibitor binds to the Q_B binding site and blocks the electron transfer from $Q_A^{\bullet-}$, leaving the charge recombination with S_2 as the only possible route for the electrons. The kinetics of $Q_A^{\bullet-}$ oxidation will, therefore, be dominated by the slow phase associated with the recombination with S_2. The addition of DCMU to both the PSIIm and the PSIIm-S/27 resulted in kinetics with very similar halftimes of ∼30 to 40 s in 50% to 60% of the centers, while the remaining 40% to 50% appear to show longer decaying times. This observation suggests that the presence of PsbS and/or Psb27 does not interfere with the DCMU binding nor the resulting inhibition. These rates are longer than those typically measured in fully functional plant PSII, where it is ∼1 s, but this is at least partially explained by the experiments being done at 15 °C to preserve the intactness of PSIIm. The slow phases of $S_2Q_A^-$ decay measured with DCMU are similar in PSIIm and PSIIm-S/27, while in the absence of DCMU, the slow phase of fluorescence decay was substantially slower in PSIIm-S/27 (Fig. 3, B and D).

A notable difference in the kinetics is shown for the PSIIm in the presence of DCMU, where an additional faster phase is present (Fig. 3D) with ∼20% amplitude and $t_{1/2} = 50$ ms. This phase could correspond to $Tyr_Z^{\bullet}Q_A^{\bullet-}$ recombination, a reaction reflecting PSII centers that lack the Mn cluster. This is consistent with the observed instability of the PSIIm.

Effect of bicarbonate on PSIIm-S/27

Given the recently discovered protective role of bicarbonate and the demonstration that it can be lost under physiological conditions (Brinkert et al. 2016), we investigated the effect of bicarbonate on PSIIm-S/27. These experiments were done at 20 °C, a temperature at which the effect of bicarbonate has been characterized and the PSIIm-S/27 was stable. The addition of 5 mM bicarbonate to the PSIIm-S/27 sample resulted in it becoming activated to a level comparable to the functional PSIIm (Fig. 4A). The kinetics of $Q_A^{\bullet-}$ oxidation after the addition of bicarbonate showed an acceleration of all 3 fluorescence decay phases to rates like those measured in the PSIIm and typical of a functional PSIIm (Zimmermann et al. 2006). In the presence of bicarbonate, the fast phase $t_{1/2}$ decreased from 67 to 3 ms, the middle phase decreased from 982 to 115 ms, and the slow phase decreased from 43 to 13 s (Table 2). The amplitude of the fast phase also appeared to increase when bicarbonate was present, but this is less certain because of the influence of the poorer fitting of the equivalent phase but with slower kinetics, in the PSIIm-S/27 lacking bicarbonate.

The addition of DCMU to the bicarbonate containing PSIIm-S/27 complex yielded almost the same kinetic profile as seen in the absence of the added 5 mM bicarbonate (Fig. 4B). The fitting of the data showed 2 main phases, the first with a halftime of ∼1 s and an amplitude of 70%, consistent with $S_2Q_A^{\bullet-}$ recombination and the second with a halftime of ∼60 s and an amplitude of 30%. The longer half-life of this second phase is consistent with the oxidation of a relatively stable donor (e.g. from Mn^{2+}, TyrD, and the side path donors) giving rise to a long-lived $Q_A^{\bullet-}$ (see e.g. Nixon et al. 1992; Debus et al. 2000).

Oxygen evolution assays performed in presence of 5 mM bicarbonate showed an ∼15-fold increase in the activity of PSIIm-S/27, reaching levels (795 ± 8 μmol O_2 mg Chl^{-1} h^{-1}) that are ∼70% of the values recorded for the PSIIm (Table 1). These results show that the PSIIm-S/27 samples contain a fully functional Mn cluster in at least 70% of the centers. Both kinetics and oxygen evolution measurements show that ∼30% of the centers lack catalytic activity and these show a kinetic profile that is consistent with either partial Mn occupancy or Mn-free PSII.

The kinetics of oxidation was studied as a function of bicarbonate concentration. The kinetics accelerated as the bicarbonate concentration was increased. When the fluorescence value at 0.2 s were plotted and the value obtained prior to the bicarbonate addition was subtracted (Fig. 4C), the curve showed hyperbolic behavior saturating at 5 mM. Data fitting with a hyperbolic model for ligand binding yielded an apparent dissociation constant for the bicarbonate of ∼600 μM.

TL (Fig. 4D) of PSIIm-S/27 with no addition showed a peak centered at 10 °C attributed to $S_2Q_A^{\bullet-}$ recombination, while in

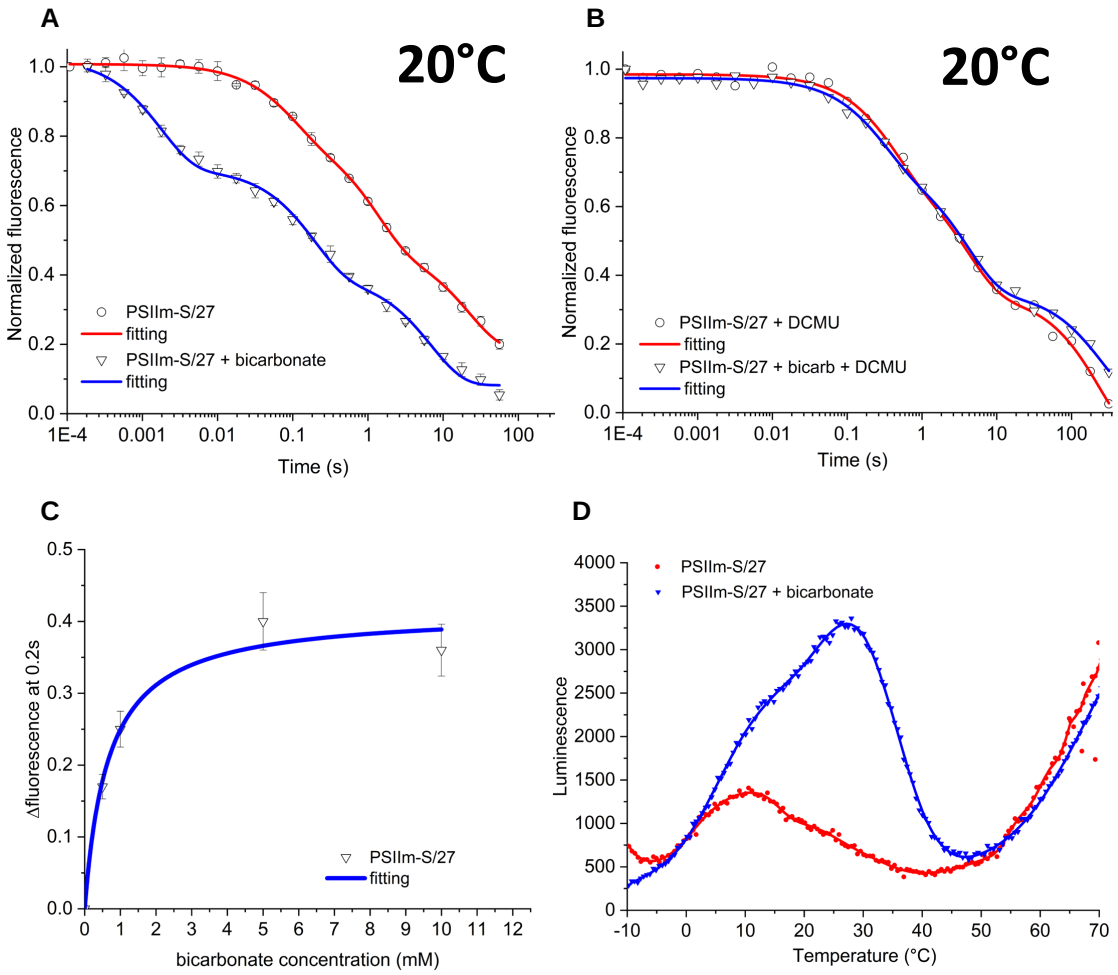

Figure 4. Effect of bicarbonate on the PSIIm-S/27 complex. **A)** Fluorescence relaxation kinetics for PSIIm-S/27, measured at 20 °C in buffer A without (circles symbols, red line) and with (triangles symbols, blue line) added 5 mM bicarbonate. Data were normalized using the initial amplitudes. Fittings were carried out with Eq. 1 (see Materials and methods). Error bars represent the SE calculated from 4 independent measurements. **B)** Fluorescence relaxation kinetics for PSIIm-S/27, measured at 20 °C in buffer A and 10 μM DCMU, without (circles symbols, red line) and with (triangles symbols, blue line) added 5 mM bicarbonate. Data were normalized using the initial amplitudes. Fittings were carried out with Eq. 1 (see Materials and methods). Error bars represent the SE calculated from 4 independent measurements. **C)** Plot of the fluorescence intensity at 0.2 s (triangles symbols) from the fluorescence relaxation kinetics, at 20 °C in buffer A, from different samples to which increasing concentrations of bicarbonate were added. The data were fitted with the hyperbole in Eq. 2 (see Materials and methods) (blue line). Error bars represent the SE calculated from 4 independent measurements; **D)** TL measurements of PSIIm-S/27 in buffer A, in the absence (red circles) and presence (blue triangles) of added 5 mM bicarbonate. Single saturating flash was given at 5 °C followed by rapid cooling to −5 °C. Scan rate was 0.5 °C/s.

the presence of bicarbonate, the TL intensity increased with a dominant peak at 27 °C, typical of $S_2Q_B^{\bullet-}$ recombination, and an increase in $S_2Q_A^{\bullet-}$ TL at 10 °C, which is seen as shoulder. The TL results show that PSIIm-S/27 has inhibited forward electron transfer from $Q_A^{\bullet-}$ and only a low level of luminescence arising from $S_2Q_A^{\bullet-}$. The addition of bicarbonate resulted in the recovery of near-normal behavior with the formation of $S_2Q_B^{\bullet-}$ recombination in most of the centers. In a fraction of centers, the bicarbonate did not reconstitute electron transfer to $Q_B^{\bullet-}$ but did result in more $S_2Q_A^{\bullet-}$ recombination.

It was also observed that the addition of 5 mM bicarbonate did not result in any substantial change in the peak intensity and position of the room temperature fluorescence spectra of a PSIIm-S/27 sample (Supplemental Fig. S3), and it did not change the elution profile of the PSIIm-S/27 in a size exclusion chromatography experiment (Supplemental Fig. S4). These observations suggest that the addition of bicarbonate does not lead to the dissociation of either PsbS or Psb27. We note that bicarbonate addition to PSIIm had no substantial effect on its activity (Table 1).

Discussion

Here, we compared 2 types of PSIIm from *N. tabacum L.*: (i) those isolated from grana, PSIIm, and (ii) those isolated from the stromal lamellae and granal margins, which contain quasi-stoichiometric amounts of PsbS and Psb27 (Table 1

and Supplemental Fig. S1), PSIIm-S/27 (Haniewicz et al. 2013, 2015). Comparison of the UV-Vis absorption and CD spectra (Figs. 2, B and D) in the 2 types of PSIIm showed only minimal differences (see Supplemental Text S2). The most substantial difference between the 2 complexes is the near absence of activity in PSIIm-S/27 compared to the high activity in the PSIIm. Both the oxygen evolution rates (Table 1) and the kinetics of $Q_A^{\bullet-}$ oxidation (Fig. 3 and Table 2) were strongly inhibited in PSIIm-S/27. The addition of DCMU to PSIIm-S/27 blocked oxygen evolution and shut down the residual, subsecond fluorescence decay, due the near-complete block of forward electron transfer from $Q_A^{\bullet-}$. The DCMU-treated PSIIm-S/27 showed 70% of the centers with the typical seconds timescale kinetics of $S_2Q_A^{\bullet-}$ recombination (Figs. 3D and 4B), while the rest of the centers showed much slower rates of $Q_A^{\bullet-}$ decay, presumably due to the electron donation from a more stable electron donor (such as Mn^{2+}, TyrD, or the donors in the cytb559 pathway) in a fraction of centers. These observations are comparable to those made by Lavergne and Leci (1993) when investigating the fraction of inactive PSII that is normally present in green algal cells. The inactive PSII in algal cells reported earlier (Lavergne and Leci 1993) could be the algal equivalent of the PSIIm-S/27 described here.

The kinetic characteristics of the impaired $Q_A^{\bullet-}$ oxidation in PSIIm-S/27 indicate heterogeneity and suggest that forward electron transfer, $Q_A^{\bullet-}$ to Q_B and to $Q_B^{\bullet-}$, and the exchange of Q_BH_2 are all inhibited. These events all involve protonation. The TL of PSIIm-S/27 had a low intensity, but the peak positions of the residual TL were consistent with inhibition of electron transfer from $Q_A^{\bullet-}$ to Q_B or $Q_B^{\bullet-}$, with the main peak at 10 °C, typical of $S_2Q_A^{\bullet-}$ recombination in inhibited centers, and only a very small shoulder at 25 °C corresponding to the $S_2Q_B^{\bullet-}$ recombination in a small number of functional centers (Fig. 3C).

The inhibition of $Q_A^{\bullet-}$ oxidation in PSIIm-S/27 cannot be explained by the loss of Q_B (except in a small fraction of the centers), as the addition of bicarbonate activated forward electron transfer in most of the centers. Similarly, the weak TL intensity cannot be explained by the absence of the Mn cluster, as most of the centers were capable of water splitting when bicarbonate was added. The low luminescence of PSIIm-S/27 prior to the addition of bicarbonate, despite the presence of the Mn cluster and both quinones, could be due to an increase in the redox potential $Q_A^{\bullet-}$, as occurs upon loss of the bicarbonate from granal PSII dimers (Brinkert et al. 2016). A sufficiently high redox potential is expected to result in the loss of radiative recombination (Rutherford et al. 2012).

The remarkable activation of the seemingly inactive PSIIm-S/27 by millimolar concentrations of bicarbonate was manifested as the appearance of normal rates of forward electron transfer and water oxidation activity in at least 70% of the centers, as monitored by fluorescence kinetics, TL, and O_2 evolution. The remaining 30% inactive centers did show a slowdown of the rate of $Q_A^{\bullet-}$ reoxidation in the ∼10 s range (Fig. 4A and Table 2). As this rate is much slower than typically found for electron transfer to Q_B and $Q_B^{\bullet-}$, this observation could indicate the absence of Q_B in the site in this fraction of the centers. However, as the 10-s phase is eliminated in the presence of DCMU and replaced by a much slower rate, ∼100 s (Fig. 4B), this behavior could indicate an unusually slow rate of electron transfer from $Q_A^{\bullet-}$ to Q_B. This could originate from a situation where the reduction potentials of $Q_A/Q_A^{\bullet-}$ and $Q_B/Q_B^{\bullet-}$ are similar. The reduction potential of $Q_A/Q_A^{\bullet-}$ is reported to shift toward that of $Q_B/Q_B^{\bullet-}$ when the Mn cluster is absent (Johnson et al. 1995), and it could be shifted even further when modified by the binding of the PsbS and Psb27 subunits.

The major difference between the 2 types of PSIIm studied here is that the PSIIm-S/27 almost completely lacks activity until activated by the addition of bicarbonate. This difference is presumably due to the binding of PsbS and/or Psb27. It is not clear which of these polypeptides is responsible for this difference or whether a combination of both is required. This uncertainty is shared with the recent structural work on other assembly intermediates in cyanobacterial systems (Huang et al. 2021; Zabert et al. 2021). Below, we discuss the potential roles of the Psb27 and PsbS.

Psb27 in land plants is relatively poorly studied and is known to exist in 2 isoforms, Psb27-1 and Psb27-2 (Chen et al. 2006; Wei et al. 2010). In the present study, it was not possible to determine which of the 2 isoforms is bound to PSIIm-S/27. Its suggested functions are associated with responses to photodamage and maturation of D1 in newly synthesized PSII (Chen et al. 2006; Wei et al. 2010). In cyanobacteria, Psb27 is involved in the assembly of the Mn_4CaO_5 cluster, where it is suggested to facilitate photoassembly by allosterically regulating the binding of the extrinsic proteins, PsbO, PsbU, and PsbV (Nowaczyk et al. 2006; Roose and Pakrasi 2008). In both *Synechocystis* sp. PCC 6803 and *Thermosynechococcus elongatus*, Psb27 was found to be associated with inactive PSIIm and dimers in which the 3 extrinsic proteins were absent and either no Mn or substoichiometric amounts of Mn were reported (Roose and Pakrasi 2004, 2008; Nowaczyk et al. 2006; Mamedov et al. 2007; Liu et al. 2011a, 2011b). Nevertheless, PSII complexes with Psb27 bound in the presence of either PsbO alone, or the full complement of extrinsic proteins, were found in a range of conditions: (i) as PSII dimers in cold-stressed *T. elongatus* (Grasse et al. 2011), (ii) in affinity purified His-tagged Psb27 in *Synechocystis* sp. PCC 6803 (Liu et al. 2011b), and (iii) as PSIIm in a *psbJ* deletion mutant of *T. elongatus* (Zabert et al. 2021).

Two recent structures of PSII complexes with bound Psb27 (Huang et al. 2021; Zabert et al. 2021) confirmed the previously suggested (Liu et al. 2011b; Komenda et al. 2012) binding site for Psb27 close to the loop E in CP43. The structures also indicate that binding of Psb27 does not directly interfere with the binding of the extrinsic proteins, in agreement with the range of different Psb27-bound forms of PSII reported in the literature, and therefore reflecting the dynamic process

of assembly and repair (Komenda et al. 2002, 2012; Roose and Pakrasi 2004, 2008; Nowaczyk et al. 2006; Mamedov et al. 2007; Grasse et al. 2011; Liu et al. 2011a, 2011b; Avramov et al. 2020; Huang et al. 2021; Zabert et al. 2021). This agrees with the observation in the present work that in the PSIIm-S/27, the Psb27 is bound, the extrinsic polypeptides are also bound, and the Mn_4CaO_5 cluster is fully assembled in the majority (70%) of the centers. It is not clear if the PSIIm-S/27 is an early-stage intermediate in the repair/assembly process, as suggested in Grasse et al. (2011) for a Mn-containing but inactive Psb27-bound PSII dimer in *T. elongatus* (Grasse et al. 2011), or a late-stage intermediate, following photoassembly of Mn cluster, prior to joining the fully functional PSII population in the grana. However, the high activity seen in PSIIm-S/27 when the centers were activated by bicarbonate points to a lack of photodamage and favors its assignment as a late-stage postphotoactivation intermediate.

The recent cryo-EM structure of the PSIIm from *T. elongatus*, showing Psb27 bound to the CP43 and no Mn cluster, also showed substantial modifications to the structure around the nonheme iron and the Q_B site. The acceptor-side modifications appear to be related to the binding of 2 other polypeptides, the Psb28 and the Psb34, that cause a conformational change of the D–E loop of the D1 protein that forms a stabilizing interaction with Psb28. Part of the C-terminus of CP47 is also displaced by Psb34 forming a stabilizing interaction with Psb28. Perhaps the most remarkable result of this conformational change was that the bicarbonate ligand to the nonheme iron was displaced by the carboxylic group of Glu241-D2 (Xiao et al. 2021; Zabert et al. 2021).

The kinetics of $Q_A^{\bullet-}$ oxidation measured for this complex (Zabert et al. 2021), and in other related complexes (Liu et al., 2011; Mamedov et al. 2007), all showed large fractions of centers with slow $Q_A^{\bullet-}$ decay (>10 s). This slow decay of $Q_A^{\bullet-}$ has been attributed to a situation in which forward electron transfer is blocked, and $Q_A^{\bullet-}$ is trapped in a long-lived state presumably due to electron donation to either $Tyr_Z^{\bullet}$ or P_{D1}^{+} in damaged centers from a stable electron donor, thus preventing $Q_A^{\bullet-}$ to from decaying by recombination. The nature of the stable, or long lived, electron donor has been hypothesized to be one of the following: cytochrome b559, $ChlZ_{D2}$ (part of the side path associated with Cytb559), or freely Mn^{2+} ions (Nixon et al. 1992; Debus et al. 2000) but could also include TyrD. This situation resembles that observed here in the fraction (~30%) of centers of PSIIm-S/27 lacking the intact Mn cluster. This fraction could represent either centers that have yet to undergo photoactivation, similarly to the intermediates presented in Zabert et al. (2021), or centers that have lost the Mn cluster during isolation from the thylakoid membrane.

Given the clear association of the Psb27 with the electron donor side in the cyanobacterial system, it is tempting to suggest that the plant Psb27 binds in a similar location and plays a similar role/s. It has been known for decades that changes on the electron donor side can have major effects on the electron acceptor side (Johnson et al. 1995). It is thus possible that the binding of the Psb27 has a long-range effect on the electron acceptor side. Indeed, in the cryoEM structure of the PSII dimer with Psb27, the Psb27 binding site overlaps with the binding site of PsbQ in plants, and PsbQ' in red algae and diatoms (Huang et al. 2021). It has been reported that the PsbQ' binding to PSII shifts the reduction potential of the $Q_A/Q_A^{\bullet-}$ couple to more positive values (Yamada et al. 2018). This suggests the possibility that the binding of Psb27 might result in a shift in the reduction potential of $Q_A/Q_A^{\bullet-}$.

There is much less relevant information for the PsbS, as there are no examples of isolated PSII cores with bound PsbS other than the PSIIm studied here (Haniewicz et al. 2013, 2015). Previous work on PsbS has been aimed at understanding its role, directly or indirectly associated with NPQ (Niyogi and Truong 2013; Ruban 2016; Bassi and Dall'Osto 2021). However, the PSIIm-S/27 was isolated from plants that had not been subjected to light stress, and therefore we do not expect that the properties of these PSIIm result from activation of NPQ mechanisms. Furthermore, the spectroscopic characterization of PSIIm-S/27 (Figs. 2 and 3) shows no quenching of the fluorescence due to PsbS binding. Therefore, a different functional role for PsbS in the PSIIm-S/27 complex should be considered. Cross-linking experiments in thylakoid membranes upon induction of quenching indicated that monomeric PsbS was associated with CP47 and D2, in addition to its expected association with LHCII (Correa-Galvis et al. 2016). The N-terminal and C-terminal loops, which are both on the stromal side of PsbS, could interact with the electron acceptor side of PSII and affect its function. In the absence of further structural information, it remains possible that the PsbS in PSIIm-S/27 is located as suggested in the cross-linking experiments (Correa-Galvis et al. 2016).

Now, we turn to the effect of bicarbonate. Here, we found that the addition of bicarbonate activated PSIIm-S/27 giving normal rates of $Q_A^{\bullet-}$ oxidation (Fig. 4A and Table 2) and oxygen evolution (Table 1) and near-normal TL (Figs. 4D and S2). This unexpected bicarbonate-dependent activation showed that the PSIIm-S/27 complex as isolated was essentially intact and capable of normal function but was "switched off." The study of the kinetics of $Q_A^{\bullet-}$ oxidation as a function of the bicarbonate concentration showed a hyperbolic dependence, typical of the binding of a ligand to a discrete binding site and an apparent dissociation constant of ~600 μM. Brinkert et al. (2016) showed that the bicarbonate binding site on the nonheme Fe in functional granal PSII dimers has 2 binding affinities: a high affinity when Q_A is present and a lower affinity when long-lived $Q_A^{\bullet-}$ is present. Based on the thermodynamic relationship between the effect of bicarbonate binding and the reduction potential (E_m) of $Q_A/Q_A^{\bullet-}$, and the literature *Kd* of 80 μM (Stemler and Murphy 1983) taken as the high affinity value, Brinkert et al. (2016) calculated the *Kd* for the low affinity state to be 1.4 mM. However, they pointed out that based on their observations, the literature *Kd* value, 80 μM, appeared to be overestimated and suggested that the actual value was in

the low micromolar range, i.e. that it had a substantial higher affinity. This would mean that the *Kd* for the low affinity conformation would be smaller than the 1.4 mM, and therefore close to, or smaller than the 600 μM *Kd* measured here for bicarbonate activation of PSIIm-S/27.

Brinkert et al. (2016) argued that the increase in the E_m of $Q_A/Q_A^{\bullet-}$ that occurred upon the loss of the bicarbonate would increase the energy gap between Pheo and Q_A, and this would disfavor the back-reaction route for charge recombination and favor direct charge recombination (Johnson et al. 1995). As described in the introduction, the back-reaction route via the pheophytin leads to chlorophyll triplet formation and thence to $^1O_2$-mediated photodamage, while the direct recombination of the slower $P^+Q_A^{\bullet-}$ radical pair is considered safe (Rutherford et al. 1982; Johnson et al. 1995). The bicarbonate-mediated redox tuning of Q_A was thus considered to be a regulatory and protective mechanism (Brinkert et al. 2016). It seems quite likely that a similar protective mechanism exists in the PSIIm-S/27, as protection is needed during and after synthesis or repair.

The increased stability of the PSIIm-S/27 conferred by the presence of PsbS and/or Psb27 was manifested by its resilience to long incubations and photochemical measurements at room temperature. This resilience contrasted with the fragility of the PSIIm, which could not be studied even for short periods at room temperature without loss of activity.

A bicarbonate-controlled, redox-tuning–based, protective mechanism in PSIIm-S/27 would appear to be beneficial for this complex. A nonfunctional PSII, like PSIIm-S/27 with an intact electron donor side but with inhibited forward electron transfer and a low-potential Q_A (Johnson et al. 1995), would be hypersensitive to back-reaction–associated photodamage, just as occurred in herbicide-treated PSII (Rutherford and Krieger-Liszkay 2001). It is known that before photoactivation of water oxidation in PSII, the E_m of $Q_A/Q_A^{\bullet-}$ is high and thus PSII is photoprotected, and at some point during the photoassembly of the Mn complex, the E_m is shifted to a functional, low-potential value (Johnson et al. 1995). If the PSIIm-S/27 is a late-stage intermediate of photoactivation, then the present work would indicate that the donor-side–induced switching of the E_m of $Q_A/Q_A^{\bullet-}$ is overridden by modifications to the acceptor side that maintain Q_A in a safe, high-potential form, until the fully assembled PSII is delivered into the granal stack and is dimerized. The binding of the PsbS and/or Psb27 can be considered as exerting conformation restrictions to the assembled but nonfunctional PSII, protecting it from photodamage until it is in the right place and dimerized. At that point, presumably the PsbS and Psb27 dissociate, allowing the PSII to adopt its functional conformation, allowing the high affinity bicarbonate site to form. The bicarbonate duly binds, shifting the E_m of $Q_A/Q_A^{\bullet-}$ to low potential and allowing optimal function. When considering the measured dissociation constant for bicarbonate in PSIIm-S/27 (600 μM), it seems clear that the physiological concentration of CO_2 could control, to some extent, the activity of this complex. At pH 8.0, the equilibrium concentration of bicarbonate will be sufficiently high to allow >50% of this complex to show normal forward electron transfer kinetics.

Another less likely explanation for the lower activity of PSIIm-S/27 is that it represents an early-stage intermediate in the repair cycle. In this model, photodamage would be manifested as an electron acceptor-side restriction, and the binding of Psb27 and/or PsbS and resulting switch to a higher potential form of Q_A due to the loss of bicarbonate would protect the system from photodamage during its transit to the repair site in the stromal lamellae.

In the literature, there are several examples of other PSII subunits which seem to exhibit similar or related effects to those described here for PsbS and Psb27, though none of them are as marked as observed in this work. These are listed in the supplementary information (Supplemental Text S3). This evidence in the literature and the present work point to a broader picture in which there is an interplay between the binding of small subunits to PSII with the resulting conformational effects and the binding of bicarbonate with the resulting redox tuning effects. This interplay appears to control electron transfer rates and thermodynamic equilibria between the different quinones in all their forms, thereby regulating and safeguarding PSII during the diverse steps of its life cycle.

Conclusions

We show that the PSIIm from the stromal lamellae/stromal margins, which has PsbS and Psb27 bound to it, has very low activity but is activated upon binding bicarbonate. These findings indicate that PSIIm-S/27 is a switched-off state that is protected from photodamage presumably due to the changes induced by the binding of either or both of the extra polypeptides. The nature of the protection mechanism appears to be complex, not least because of sample heterogeneity, but the dominant mechanism in the PSIIm-S/27 sample appears to involve a modification of the Q_B site, affecting its proton-coupled electron transfer properties and its exchange with the PQ pool. Another important feature of this complex is the diminished affinity for bicarbonate and the notable positive redox shift of the $Q_A/Q_A^{\bullet-}$ reduction potential that appears to be present when the bicarbonate is not bound. Just such a shift occurs in standard granal PSII dimers when bicarbonate is released upon $Q_A^{\bullet-}$ accumulation (Brinkert et al. 2016). The redox shift protects against the well-characterized photodamage arizing from chlorophyll triplet-mediated, singlet-oxygen generation by favoring a direct recombination route for $P^{\bullet+}Q_A^{\bullet-}$ (Johnson et al. 1995). This kind of protection is expected to be important in a near-intact PSII that is switched-off in transit, either after photoactivation or prior to repair.

Materials and methods

Growth and cultivation of tobacco plants

Transplastomic plants of tobacco (*N. tabacum* L.), which have a hexa-histidine tag sequence at the 5′ end of the

gene coding for the PsbE subunit, were used for this work (Fey et al. 2008). Plants were kept at a constant temperature of 25 °C, at 50% relative humidity, and grown for 10 to 12 wk under a light regime of 12 h/d, with a light intensity of 150 to 200 μmol photons s^{-1} m^{-2}.

Thylakoids preparation and PSII core solubilizations

Thylakoid membranes and PSII cores were prepared as previously reported (Haniewicz et al. 2013, 2015), with only minimal modifications in the solubilization step. Briefly, PSII core complexes retaining the subunits PsbS and Psb27 were obtained from thylakoid membranes solubilized for 5 min at 4 °C at a final chlorophyll concentration of 3 mg/mL. After solubilization, the unsolubilized fraction was separated by centrifugation at 35,000 × *g* for 10 min at 4 °C. The unsolubilized fraction underwent a second solubilization step to isolate the PSII core complexes lacking PsbS and Psb27. This second solubilization took place for 15 min at 4 °C at a final chlorophyll concentration of 1 mg/mL. Also, after this second solubilization, the unsolubilized fraction was separated by centrifugation at 35,000 × *g* for 10 min at 4 °C. In both cases, the solubilization was carried out in the dark, adjusting the chlorophyll concentration with grinding buffer (20 mM MES–NaOH, pH 6.5, and 5 mM $MgCl_2$) and using 20 mM (1.02% *w*/*v*) n-dodecyl-β-D-maltoside (β-DDM).

PSII core complexes isolation

Photosystem II samples were prepared using Ni-affinity chromatography and a subsequent step of size exclusion chromatography as reported in Haniewicz et al. (2013) for PSII complexes retaining the subunit PsbS and according to Haniewicz et al. (2015) for PSII complex lacking the subunit PsbS. For the size exclusion chromatography step, buffer contains 20 mM MES–NaOH, pH 6.5, 20 mM NaCl, 5 mM $MgCl_2$, 1 mM $CaCl_2$, 10 mM $NaHCO_3$, and 0.02% w/v (~0.39 mM) β-DDM. Previously, a slightly higher detergent content was used of 0.03% (~0.59 mM) (Haniewicz et al. 2013, 2015). In these studies, all chromatography columns were subjected to the ReGenFix procedure (https://www.regenfix.eu/) for regeneration and calibration prior use.

Polyacrylamide gel electrophoresis

Denaturing SDS–PAGE consisted 10% (*w*/*v*) separating polyacrylamide/urea gels with 4% (*w*/*v*) stacking gels (Piano et al. 2010; Collu et al. 2017). Samples were denatured with Roti Load (Roth) at room temperature before loading, and, after electrophoresis gels were stained with Coomassie Brilliant Blue G250.

Absorption, CD spectroscopy, and chlorophyll determination

The protein content of thylakoids was assessed through 3 independent measurements based on the concentrations of chlorophyll *a* and chlorophyll *b*. The absorption of chlorophylls extracted in 80% (*v*/*v*) acetone, in a dilution factor of 200 or 500, was measured with a Pharmacia Biotech Ultrospec 4000 spectrophotometer, and their relative concentrations were calculated according to Porra et al. (1989). CD spectra were the average of 3 accumulations recorded at a sensitivity of 100 mdeg and a scan speed of 100 nm/min using a CD spectrometer JASCO J-810. Absorption and CD spectra were recorded at room temperature in the range of 370 to 750 nm, with an optical path length of 1 cm and a bandpass of 2 nm. Spectra were recorded on an absorption Ultra Micro quartz cell with 10-mm light path (Hellma Analytics). In all cases, measurements were performed in a range between 0.01 and 0.2 mg/mL Chls, and samples were diluted in buffer containing 20 mM MES–NaOH, pH 6.5, 5 mM $MgCl_2$, 1 mM $CaCl_2$, and 0.02% *w*/*v* (~0.39 mM) β-DDM (buffer A).

Fluorescence spectroscopy and kinetics

Emission and excitation spectra were recorded on a Jasco FP-8200 spectrofluorometer at 4 °C in 0.1-nm steps and 3-nm bandpass. Spectra were corrected for the photomultiplier sensitivity using a calibrated lamp spectrum. Emission spectra in the range of 600 to 750 nm were recorded using the main absorption bands as excitation wavelength (437 nm in Fig. 2). Fluorescence spectra were recorded on a fluorescence Ultra Micro quartz cell with 3-mm light path (Hellma Analytics). The flash-induced increase and the subsequent decay of chlorophyll fluorescence yield, and the values of F_0, F_m, and F_v were measured with a fast double modulation fluorimeter (FL 3000, PSI, Czech Republic). The sample concentration was 5 μg Chl/mL in buffer A. For experiments on bicarbonate effects, samples were suspended in buffer A but lacking $CaCl_2$ (buffer B). Samples were subjected to a preillumination in room light for 10 s followed by a period of 5 to 10 min of dark adaptation.

Multicomponent deconvolution of the measured curves was done by using a fitting function with 3 components based on the widely used model of the 2-electron gate (Crofts and Wraight 1983; Vass et al. 1999). The fast and middle phases were simulated with exponential components. However, slow recombination of $Q_A^{\bullet-}$ via charge recombination has been shown to obey hyperbolic kinetics corresponding to an apparently second-order process (Bennoun 1994), most probably the result of stretched exponentials indicative of inhomogeneity in this time range. Therefore, the data were fitted with a linear combination of 2 exponentials and a hyperbolic component, where $F_{(t)}$ is the variable fluorescence yield, F_0 is the basic fluorescence level before the flash, A_1–A_3 are the amplitudes, T_1–T_3 are the time constants, from which the half-lives were calculated via $t_{1/2} = \ln 2 \cdot T$ for the exponential components, and $t_{1/2}$ is the T for the hyperbolic component.

$$F_{(t)} - F_{(0)} = A_1 \exp(-t/T_1) + \boldsymbol{A}_2 \exp(-t/T_2) + A_3/(1 + t/T_3). \quad (1)$$

When the herbicide DCMU was added, 10 μM of an ethanolic solution was added in the dark to 1 mL of protein solution in buffer B, prior to the 5-min dark adaptation step.

The kinetics measured as a function of increasing concentrations of bicarbonate (0.5, 1, 5, and 10 mM) were fitted with a hyperbolic curve (Eq. 2) from which the apparent dissociation constant ($K_{d\ app}$) was calculated.

$$\Delta\text{Fluorescence at } 0.2\text{ s} = f_{max}/(K_{d_{app}} + [\text{bicarbonate}]), \quad (2)$$

where ΔFluorescence at 0.2 s is the difference in fluorescence value at 0.2 s subtracted of the value before any addition of bicarbonate and f_{max} is the fluorescence difference value when the binding site is fully occupied. The pH was monitored upon addition of bicarbonate to make sure that no shifts in pH occurred.

Due to the equilibrium between bicarbonate/carbonate and CO_2 and its pH dependence, additions of bicarbonate were performed in a sealable cuvette. Upon addition of bicarbonate, the cuvette was sealed with a screw cap with minimum or no headspace to limit any shift in the equilibrium toward gaseous CO_2. Furthermore, the measurements were performed within minutes of the addition to preserve bicarbonate at the concentration added.

Oxygen evolution

The oxygen evolution was measured with a Clark-type electrode (Hansatech, England) at 20 °C, with 1 mM 2,6-dichloro-p-benzoquinone and 1 mM ferricyanide as electron acceptors in the reaction mixture. Measurements were carried on samples with a chlorophyll concentration of 1 mg/mL diluted 20 times in buffer A (12 mM Cl^- and 1 mM Ca^{2+} maintain activity in PSII lacking PsbQ and or PsbP) to a final concentration of 50 μg Chl/mL. Three independent measurements were done on the same preparation to test the activity. Reactions were started with illumination from a white light source (400 to 700 nm) with a PPFD of 700 to 800 μmoles of photons m^{-2} s^{-1}. For the effect of bicarbonate on PSIIm and PSIIm-S/27 samples, 5 mM $NaHCO_3$ was added to the reaction mixture just before the measurement. Oxygen measurements with the Clark-type setup rely on avoiding any equilibration between the sample and the external atmosphere. We therefore expect that in this experimental setup, changes in bicarbonate concentrations due to the equilibrium between bicarbonate/carbonate and carbonic acid and CO_2 will be negligible.

Thermoluminescence

TL was measured with a lab-built apparatus, essentially as described in Ducruet and Vass (2009) but using a GaAsP photomultiplier H10769A-50 (Hamamatsu). Samples were preilluminated with room light (~20 μmol m^{-2} s^{-1}) for 10 s, dark-adapted for 5 to 10 min, and then cooled to 5 °C. After 2 min, samples were excited with a single turnover saturating flash. Finally, samples were rapidly cooled to −15 °C, and luminescence was recorded with a 20 °C/min heating rate. The sample concentration was 5 μg Chl/mL in buffer B. Bicarbonate was added immediately before freezing the sample to −15 °C.

Accession numbers

Sequence data from this article can be found in the Uniprot library (*N. tabacum* entries). The main proteins mentioned in this manuscript are under accession numbers Q9SMB4 (PsbS), A0A1S4DN09, and A0A1S4DRV5 (Psb27).

Acknowledgments

We thank J.-M. Ducruet for help with setting up the TL. We thank Miss M.B. Farci for the kind help with the Fig. 1 by providing the original drawing of thylakoid membranes.

Author contributions

A.F., A.W.R., D.P., and C.B. designed research; A.F., K.P., D.P., P.H., and D.F. performed research; D.P. and D.F. contributed new reagents/analytic tools; A.F., K.P., A.W.R., C.B., M.B., and D.P. analyzed data; and A.F. A.W.R., D.P., P.H., D.F., C.B., M.B., and M.C.L. wrote the paper.

Supplemental data

The following materials are available in the online version of this article.

Supplemental Figure S1. Comparisons of the PSIIm and PSIIm-S/27.

Supplemental Figure S2. Fitting of the TL data for PSIIm-S/27 in the absence (red circles) and presence (blue triangles) of 5 mM bicarbonate.

Supplemental Figure S3. Room temperature fluorescence for PSIIm-S/27 in the absence (red line) and presence (blue line) of added 5 mM bicarbonate.

Supplemental Figure S4. The effect of bicarbonate on the retention of PsbS and Psb27 in PSIIm-S/27 samples analyzed by size exclusion chromatography (SEC).

Supplemental Table S1. Mass spectrometry analysis of PSIIm and PSIIm-S/27.

Supplemental Text S1.

Supplemental Text S2.

Supplemental Text S3.

Funding

This work was carried out with the support of the program Homing Plus (Foundation for Polish Science) grant no. 2012-6/10 cofinanced by the European Union under the European Regional Development Funds (to D.P.), the PRELUDIUM programme (National Science Centre) grant

number DEC-2012/05/05/N/NZ1/01922 (to P.H.), and the Biotechnology and Biological Sciences Research Council (BBSRC) grants BB/K002627/1 and BB/R00921X (to A.W.R.).

Conflict of interest statement. The authors declare no conflict of interest.

Data Availability

All materials available upon request.

References

Albertsson P-A. A quantitative model of the domain structure of the photosynthetic membrane. Trends in Plant Sci. 2001:**6**(8):349–354. https://doi.org/10.1016/S1360-1385(01)02021-0

Alfonso M, Montoya G, Cases R, Rodríguez R, Picorel R. Core antenna complexes, CP43 and CP47, of higher plant photosystem II. Spectral properties, pigment stoichiometry, and amino acid composition. Biochem. 1994:**33**(34):10494–10500. https://doi.org/10.1021/bi00200a034

Andersson B, Anderson J-M. Lateral heterogeneity in the distribution of chlorophyll-protein complexes of the thylakoid membranes of spinach chloroplasts. Biochim Biophys Acta. 1980:**593**(2):427–440. https://doi.org/10.1016/0005-2728(80)90078-X

Avramov AP, Hwang HJ, Burnap RL. The role of Ca^{2+} and protein scaffolding in the formation of nature's water oxidizing complex. Proc Natl Ac Sci U S A. 2020:**117**(45):28036–28045. https://doi.org/10.1073/pnas.2011315117

Bassi R, Dall'Osto L. Dissipation of light energy absorbed in excess: the molecular mechanisms. Annu Rev Plant Biol. 2021:**72**(1):47–76. https://doi.org/10.1146/annurev-arplant-071720-015522

Bennoun P. Chlororespiration revisited: mitochondrial-plastid interactions in *Chlamydomonas*. Biochim Biophys Acta. 1994:**1186**(1-2):59–66. https://doi.org/10.1016/0005-2728(94)90135-X

Bergantino E, Segalla A, Brunetta A, Teardo E, Rigoni F, Giacometti GM, Szabò I. Light- and pH-dependent structural changes in the PsbS subunit of photosystem II. Proc Natl Acad Sci U S A. 2003:**100**-(25):15265–15270. https://doi.org/10.1073/pnas.2533072100

Brinkert K, De Causmaecker S, Krieger-Liszkay A, Fantuzzi A, Rutherford AW. Bicarbonate-induced redox tuning in photosystem II for regulation and protection. Proc Natl Acad Sci U S A. 2016:**113**-(43):12144–12149. https://doi.org/10.1073/pnas.1608862113

Caffarri S, Kouril R, Kereïche S, Boekema EJ, Croce R. Functional architecture of higher plant photosystem II supercomplexes. EMBO J. 2009:**28**(19):3052–3063. https://doi.org/10.1038/emboj.2009.232

Chen H, Zhang D, Guo J, Wu H, Jin M, Lu Q, Lu C, Zhang L. A Psb27 homologue in *Arabidopsis thaliana* is required for efficient repair of photodamaged photosystem II. Plant Mol Biol. 2006:**61**(4-5):567–575. https://doi.org/10.1007/s11103-006-0031-x

Collu G, Farci D, Esposito F, Pintus F, Kirkpatrick J, Piano D. New insights into the operative network of FaEO, an enone oxidoreductase from *Fragaria x ananassa* Duch. Plant Mol Biol. 2017:**94**(1-2):125–136. https://doi.org/10.1007/s11103-017-0597-5

Correa-Galvis V, Poschmann G, Melzer M, Stühler K, Jahns P. PsbS interactions involved in the activation of energy dissipation in *Arabidopsis*. Nat Plants 2016:**2**(2):15225. https://doi.org/10.1038/nplants.2015.225

Crofts AR, Wraight CA. The electrochemical domain of photosynthesis. Biochim Biophys Acta. 1983:**726**(3):149–185. https://doi.org/10.1016/0304-4173(83)90004-6

Danielsson R, Suorsa M, Paakkarinen V, Albertsson P-A, Styring S, Aro E-M, Mamedov F. Dimeric and monomeric organization of photosystem II. J Biol Chem 2006:**281**(20):14241–14249. https://doi.org/10.1074/jbc.M600634200

Dau H, Zaharieva I. Principles, efficiency, and blueprint character of solar-energy conversion in photosynthetic water oxidation. Acc Chem Res. 2009:**42**(12):1861–1870. https://doi.org/10.1021/ar900225y

Debus RJ, Campbell KA, Pham DP, Hays A-MA, Britt RD. Glutamine 189 of the D1 polypeptide modulates the magnetic and redox properties of the manganese cluster and tyrosine Y_Z in photosystem II. Biochem. 2000:**39**(21):6275–6287. https://doi.org/10.1021/bi992749w

De Causmaecker S, Douglass JS, Fantuzzi A, Nitschke N, Rutherford AW. Energetics of the exchangeable quinone, Q_B, in photosystem II. Proc Natl Acad Sci. 2019:**116**(39):19458–19463. https://doi.org/10.1073/pnas.1910675116

Dietzel L, Bräutigam K, Steiner S, Schüffler K, Lepetit B, Grimm B, Schöttler MA, Pfannschmidt T. Photosystem II supercomplex remodelling serves as an entry mechanism for state transitions in *Arabidopsis*. Plant Cell 2011:**23**(8):2964–2977. https://doi.org/10.1105/tpc.111.087049

Ducruet J, Vass I. Thermoluminescence: experimental. Photosynth Res. 2009:**101**(2-3):195–204. https://doi.org/10.1007/s11120-009-9436-0

Fan M, Li M, Liu Z, Cao P, Pan X, Zhang H, Zhao X, Zhang J, Chang W. Crystal structures of the PsbS protein essential for photoprotection in plants. Nat Struct Mol Biol 2015:**22**(9):729–735. https://doi.org/10.1038/nsmb.3068

Fey H, Piano D, Horn R, Fischer D, Schmidt M, Ruf S, Schröder WP, Bock R, Büchel C. Isolation of highly active photosystem II core complexes with a His-tagged Cyt b_{559} subunit from transplastomic tobacco plants. Biochim Biophys Acta. 2008:**1777**(12):1501–1509. https://doi.org/10.1016/j.bbabio.2008.09.012

Gachek DA, Holleboom CP, Tietz S, Kirchhoff H, Walla PJ. PsbS-dependent and -independent mechanisms regulate carotenoid-chlorophyll energy coupling in grana thylakoids. FEBS Lett. 2019:**593**-(22):3190–3197. https://doi.org/10.1002/1873-3468.13586

Grasse N, Mamedov F, Becker K, Styring S, Rögner M, Nowaczyk MM. Role of novel dimeric photosystem II (PSII)-Psb27 protein complex in PSII repair. J of Biol Chem. 2011:**286**(34):29548–29555. https://doi.org/10.1074/jbc.M111.238394

Haniewicz P, De Sanctis D, Büchel C, Schröder W P, Loi M C, Kieselbach T, Bochtler M, Piano D. Isolation of monomeric photosystem II that retains the subunit PsbS. Photosynth Res. 2013:**118**(3):199–207. https://doi.org/10.1007/s11120-013-9914-2

Haniewicz P, Floris D, Farci D, Kirkpatrick J, Loi MC, Büchel C, Bochtler M, Piano D. Isolation of plant photosystem II complexes by fractional solubilization. Front Plant Sci. 2015:**6**:1100. https://doi.org/10.3389/fpls.2015.01100

Huang G, Xiao Y, Pi X, Zhao L, Zhu Q, Wang W, Kuang T, Han G, Sui SF, Shen JR. Structural insights into a dimeric Psb27-photosystem II complex from a cyanobacterium *Thermosynechococcus vulcanus*. Proc Natl Acc Sci U S A. 2021:**118**(5):e2018053118. https://doi.org/10.1073/pnas.2018053118

Johnson MP. Photosynthesis. Essays Biochem. 2016:**60**(3):255–273. https://doi.org/10.1042/EBC20160016

Johnson GN, Rutherford AW, Krieger A. A change in the midpoint potential of the quinone Q(A) in photosystem II associated with photoactivation of oxygen evolution. Biochim Biophys Acta. 1995:**1229**(2):202–207. https://doi.org/10.1016/0005-2728(95)00003-2

Kirchhoff H. Chloroplast ultrastructure in plants. New Phytologist. 2019:**223**(2):565–574. https://doi.org/10.1111/nph.15730

Komenda J, Lupinkova L, Kopecky J. Absence of the *psbH* gene product destabilizes photosystem II complex and bicarbonate binding on its acceptor side in *Synechocystis* PCC 6803. Eur J Biochem 2002:**269**(2):610–619. https://doi.org/10.1046/j.0014-2956.2001.02693.x

Komenda J, Sobotka R, Nixon PJ. Assembling and maintaining the photosystem II complex in chloroplasts and cyanobacteria. Curr Op in Plant Biol. 2012:**15**(3):245–251. https://doi.org/10.1016/j.pbi.2012.01.017

Krausz E, Hughes JL, Smith P, Pace R, Årsköld SP. Oxygen-evolving photosystem II core complexes: a new paradigm based on the spectral identification of the charge-separating state, the primary acceptor and assignment of low-temperature fluorescence. Photochem Photobiol Sci 2005:**4**(9):744–753. https://doi.org/10.1039/b417905f

Krieger-Liszkay A. Singlet oxygen production in photosynthesis. J of Exp Bot. 2005:**56**(411):337–346. https://doi.org/10.1093/jxb/erh237

Lavergne J, Leci E. Properties of inactive photosystem II centres. Photosynth Res. 1993:**35**(3):323–343. https://doi.org/10.1007/BF00016563

Li XP, Gilmore AM, Caffarri S, Bassi R, Golan T, Kramer D, Niyogi KK. Regulation of photosynthetic light harvesting involves intrathylakoid lumen pH sensing by the PsbS protein. J Biol Chem. 2004:**279**(22):22866–22874. https://doi.org/10.1074/jbc.M402461200

Liguori N, Campos SRR, Baptista AM, Croce R. Molecular anatomy of plant photoprotective switches: the sensitivity of PsbS to the environment, residue by residue. J Phys Chem Lett. 2019:**10**(8):1737–1742. https://doi.org/10.1021/acs.jpclett.9b00437

Liu H, Roose JL, Cameron JC, Pakrasi HB. A genetically tagged Psb27 protein allows purification of two consecutive photosystem II (PSII) assembly intermediates in *Synechocystis* 6803, a cyanobacterium. J of Biol Chem. 2011a:**286**(28):24865–24871. https://doi.org/10.1074/jbc.M111.246231

Liu HJ, Huang RYC, Chen JW, Gross ML, Pakrasi HB. Psb27, a transiently associated protein, binds to the chlorophyll binding protein CP43 in photosystem II assembly intermediates proc. Natl Acad Sci U S A. 2011b:**108**(45):18536–18541. https://doi.org/10.1073/pnas.1111597108

Ljungberg U, Åkerlund HE, Larsson C, Andersson B. Identification of polypeptides associated with the 23 and 33 kDa proteins of photosynthetic oxygen evolution. Biochim Biophys Acta. 1984:**767**(1):145–152. https://doi.org/10.1016/0005-2728(84)90089-6

Mamedov F, Nowaczyk MM, Thapper A, Rogner M, Styring S. Functional characterization of monomeric photosystem II core preparations from *Thermosynechococcus elongatus* with or without the Psb27 protein. Biochem. 2007:**46**(18):5542–5551. https://doi.org/10.1021/bi7000399

Melis A. Functional properties of photosystem II_β in spinach chloroplasts. Biochim Biophys Acta. 1985:**808**(2):334–342. https://doi.org/10.1016/0005-2728(85)90017-9

Nickelsen J, Rengstl B. Photosystem II assembly: from cyanobacteria to plants. Annu Rev Plant Biol. 2013:**64**(1):609–635. https://doi.org/10.1146/annurev-arplant-050312-120124

Nixon PN, Trost JT, Diner BA. Role of carboxyl terminus of polypeptide D1 in the assembly of a functional water-oxidizing manganese cluster in photosystem II of the cyanobacterium *Synechocystis* sp. PCC 6803: assembly requires a free carboxyl group at C-terminal position 344. Biochem. 1992:**31**(44):10859–10871. https://doi.org/10.1021/bi00159a029

Niyogi KK, Truong TB. Evolution of flexible non-photochemical quenching mechanisms that regulate light harvesting in oxygenic photosynthesis. Curr Op Plant Biol. 2013:**16**(3):307–314. https://doi.org/10.1016/j.pbi.2013.03.011

Nowaczyk MM, Hebeler R, Schlodder E, Meyer HE, Warscheid B, Rögner M. Psb27, a cyanobacterial lipoprotein, is involved in the repair cycle of photosystem II. Plant Cell 2006:**18**(11):3121–3131. https://doi.org/10.1105/tpc.106.042671

Piano D, El Alaoui S, Korza HJ, Filipek R, Sabala I, Haniewicz P, Buechel C, De Sanctis D, Bochtler M. Crystallization of the photosystem II core complex and its chlorophyll binding subunit CP43 from transplastomic plants of *Nicotiana tabacum*. Photosynth Res. 2010:**106**(3):221–226. https://doi.org/10.1007/s11120-010-9597-x

Porra RJ, Thompson WA, Kriedmann PE. Determination of accurate extinction coefficients and simultaneous equations for assaying chlorophylls *a* and *b* with four different solvents: verifications of the concentration of chlorophyll standards by atomic absorption spectroscopy. Biochim Biophys Acta. 1989:**975**(3):384–394. https://doi.org/10.1016/S0005-2728(89)80347-0

Pospíšil P. Production of reactive oxygen species by photosystem II as a response to light and temperature stress. Front Plant Sci. 2016:**7**:1950. https://doi.org/10.3389/fpls.2016.01950

Puthiyaveetil S, Tsabari O, Lowry T, Lenhert S, Lewis RR, Reich Z, Kirchhoff H. Compartimentalization of the protein repair machinery in photosynthetic membrane. Proc Natl Acad Sci U S A. 2014:**111**-(44):15839–15844. https://doi.org/10.1073/pnas.1413739111

Roach T, Krieger-Liszkay A. The role of the PsbS protein in the protection of Photosystems I and II against high light in *Arabidopsis thaliana*. Biochim Biophys Acta. 2012:**1817**(12):2158–2165. https://doi.org/10.1016/j.bbabio.2012.09.011

Roose JL, Pakrasi HB. Evidence that D1 processing is required for manganese binding and extrinsic protein assembly into photosystem II. J Biol Chem 2004:**279**(44):45417–45422. https://doi.org/10.1074/jbc.M408458200

Roose JL, Pakrasi HB. The Psb27 protein facilitates manganese cluster assembly in photosystem II. J Biol Chem 2008:**283**(7):4044–4050. https://doi.org/10.1074/jbc.M708960200

Ruban AV. Nonphotochemical chlorophyll fluorescence quenching: mechanism and effectiveness in protecting plants from photodamage. Plant Physiol. 2016:**170**(4):1903–1916. https://doi.org/10.1104/pp.15.01935

Ruban AV, Johnson MP. Visualizing the dynamic structure of the plant photosynthetic membrane. Nat Plants 2015:**1**(11):15161. https://doi.org/10.1038/nplants.2015.161

Rutherford AW, Crofts AR, Inoue Y. Thermoluminescence as a probe of photosystem II photochemistry: the origin of the flash induced glow peaks. Biochim Biophys Acta. 1982:**682**(3):457–465. https://doi.org/10.1016/0005-2728(82)90061-5

Rutherford AW, Krieger-Liszkay A. Herbicide-induced oxidative stress in photosystem II. Trends In Biochem Sc. 2001:**26**(11):648–653. https://doi.org/10.1016/S0968-0004(01)01953-3

Rutherford AW, Osyczka A, Rappaport F. Back-reactions, short-circuits, leaks and other energy wasteful reactions in biological electron transfer: redox tuning to survive life in O_2. FEBS Lett. 2012:**586**(5):603–616. https://doi.org/10.1016/j.febslet.2011.12.039

Rutherford AW, Paterson DR, Mullet JE. A light-induced spin-polarized triplet detected by EPR in photosystem II reaction centers. Biochim Biophys Acta. 1981:**635**(2):205–214. https://doi.org/10.1016/0005-2728(81)90020-7

Sacharz J, Giovagnetti V, Ungerer P, Mastroianni G, Ruban AV. The xanthophyll cycle affects reversible interactions between PsbS and light-harvesting complex II to control non-photochemical quenching. Nat Plant. 2017:**3**(2):16225. https://doi.org/10.1038/nplants.2016.225

Shevela D, Eaton-Rye JJ, Shen JR, Govindjee . Photosystem II and the unique role of bicarbonate: a historical perspective. Biochim Biophys Acta. 2012:**1817**(8):1134–1151. https://doi.org/10.1016/j.bbabio.2012.04.003

Stemler A, Murphy J. Determination of the binding constant of $H^{14}CO_3^-$ to the photosystem II complex in maize chloroplasts—effects of inhibitors and light. Photochem Photobiol 1983:**38**(6):701–707. https://doi.org/10.1111/j.1751-1097.1983.tb03603.x

Tikkanen M, Aro EM. Thylakoid protein phosphorylation in dynamic regulation of photosystem II in higher plants. Biochim Biophys Acta. 2012:**1817**(1):232–238. https://doi.org/10.1016/j.bbabio.2011.05.005

Tomizioli M, Lazar C, Brugière S, Burger T, Salvi D, Gatto L, Moyet L, Breckels LM, Hesse A-M, Lilley K-S, et al. Deciphering thylakoid sub-compartments using a mass spectrometry-based approach. Mol Cell Proteomics. 2014:**13**(8):2147–2167. https://doi.org/10.1074/mcp.M114.040923

Vass I, Kirilovsky D, Etienne A-L. UV-B radiation-induced donor- and acceptor-side modifications of photosystem II in the cyanobacterium *Synechocystis* sp. PCC 6803. Biochem. 1999:**38**(39):12786–12794. https://doi.org/10.1021/bi991094w

Vothknecht U C, Westhoff P. Biogenesis and origin of thylakoid membranes. Biochim Biophys Acta. 2002:**1541**(1-2):91–101. https://doi.org/10.1016/S0167-4889(01)00153-7

Ware MA, Giovagnetti V, Belgio E, Ruban AV. PsbS protein modulates non-photochemical chlorophyll fluorescence quenching in membranes depleted of photosystems. J Photochem Photobiol B. 2015:**152**(part B):301–307. https://doi.org/10.1016/j.jphotobiol.2015.07.016

Watanabe M, Iwai M, Narikawa R, Ikeuchi M. Is the photosystem II complex a monomer or a dimer? Plant Cell Physiol. 2009:**50**(9):1674–1680. https://doi.org/10.1093/pcp/pcp112

Wei L, Guo J, Ouyang M, Sun X, Ma J, Chi W, Lu C, Zhang L. LPA19, a Psb27 homolog in *Arabidopsis thaliana*, facilitates D1 protein precursor processing during PSII biogenesis. J Biol Chem 2010:**285**(28):21391–21398. https://doi.org/10.1074/jbc.M110.105064

Xiao Y, Huang G, You X, Zhu Q, Wang W, Kuang T, Han G, Sui SF, Shen JR. Structural insights into cyanobacterial photosystem II intermediates associated with Psb28 and Tsl0063. Nat Plants 2021:**7**(8):1132–1142. https://doi.org/10.1038/s41477-021-00961-7

Yamada M, Nagao R, Iwai M, Arai Y, Makita A, Ohta H, Tomo T. The PsbQ′ protein affects the redox potential of the Q_A in photosystem II. Photosynthetica 2018:**56**(SPECIAL ISSUE):185–191. https://doi.org/10.1007/s11099-018-0778-8

Zabert J, Bohn S, Schuller SK, Arnolds O, Möller M, Meier-Credo J, Liauw P, Chan A, Tajkhorshid E, Langer JD, et al. Structural insights into a photosystem II assembly. Nat Plants 2021:**7**(4):524–538. https://doi.org/10.1038/s41477-021-00895-0

Zimmermann K, Heck M, Frank J, Kern J, Vass I, Zouni A. Herbicide biding and thermal stability of photosystem II isolated from *Thermosynechococcus elongatus*. Biochim Biophys Acta. 2006:**1757**(2):106–114. https://doi.org/10.1016/j.bbabio.2005.12.002